

# Bronchial epithelial transcriptome reveals dysregulated interferon and inflammatory responses to rhinovirus in exacerbation-prone pediatric asthma

Naresh Doni Jayavelu,<sup>1</sup> Basilin Benson,<sup>1</sup> Patricia C. dela Cruz,<sup>2</sup> Weston T. Powell,<sup>2,3</sup> Lucille M. Rich,<sup>2</sup> Elizabeth R. Vanderwall,<sup>2</sup> Camile R. Gates,<sup>2</sup> Andrew J. Nagel,<sup>4</sup> Maria P. White,<sup>2</sup> Nyssa B. Samanas,<sup>2</sup> Kourtne Whitfield,<sup>5</sup> Teal S. Hallstrand,<sup>6</sup> Steven F. Ziegler,<sup>1</sup> Matthew C. Altman,<sup>1,4</sup> and Jason S. Debley<sup>2,3</sup>

<sup>1</sup>Systems Immunology Division, Benaroya Research Institute at Virginia Mason, Seattle, Washington, USA. <sup>2</sup>Center for Respiratory Biology and Therapeutics, Seattle Children's Research Institute, Seattle, Washington, USA. <sup>3</sup>Department of Pediatrics, Division of Pulmonary and Sleep Medicine, Seattle Children's Hospital, University of Washington, Seattle, Washington, USA. <sup>4</sup>Division of Allergy and Infectious Diseases, University of Washington School of Medicine, Seattle, Washington, USA. <sup>5</sup>School of Biological Sciences, Washington State University, Pullman, Washington, USA. <sup>6</sup>Center for Lung Biology, Division of Pulmonary, Critical Care and Sleep Medicine, University of Washington, Seattle, Washington, USA.

**Host factors influencing susceptibility to rhinovirus-induced asthma exacerbations remain poorly characterized. Using organotypic bronchial epithelial cultures from well-characterized children with asthma and healthy children, this study investigated viral load kinetics and resultant host responses by bulk and single-cell transcriptomics and targeted protein analyses. Bronchial epithelium from exacerbation-prone children exhibited greater rhinovirus replication and a cascade of exaggerated downstream interferon (IFN), inflammatory, epithelial stress, and remodeling responses. These transcriptional patterns were confirmed and further refined using single-cell transcriptomics, revealing cell type-specific contributions – particularly from non-ciliated cell populations including secretory immune response, tuft, and basal cells. We observed that these post-infection differences were associated with lower pre-infection IFN-stimulated gene (ISG) expression and protein levels of the ISG CXCL10. Prophylactic IFN- $\beta$  treatment reduced viral replication and normalized downstream responses, supporting low baseline (pre-infection) IFN tone as a modifiable causal determinant of host susceptibility to adverse rhinovirus-induced responses in exacerbation-prone children with asthma.**

**Authorship note:** NDJ and BB contributed equally to this work and have been designated as co-first authors. MCA and JSD contributed equally to this work and have been designated as co-senior authors.

**Conflict of interest:** The authors have declared that no conflict of interest exists.

**Copyright:** © 2025, Doni Jayavelu et al. This is an open access article published under the terms of the Creative Commons Attribution 4.0 International License.

**Submitted:** July 8, 2025

**Accepted:** November 4, 2025

**Published:** November 11, 2025

**Reference information:** *JCI Insight*. 2025;10(24):e197711.  
<https://doi.org/10.1172/jci.insight.197711>.

## Introduction

Viral infections are the primary trigger of up to 90% of asthma exacerbations in children, with rhinoviruses (RVs) being the most strongly associated with exacerbations (1, 2). Host factors influencing the risk of RV-triggered exacerbations remain poorly characterized. Early studies suggested that primary bronchial epithelial cells (BECs) from asthma donors had deficient type I and/or III interferon (IFN) responses to RV (3, 4) and postulated that deficient epithelial IFN responses to viruses may predispose to exacerbations. However, this concept remained controversial over the past two decades as later studies did not report differences in epithelial IFN responses to viruses between asthma and healthy donors (5, 6). More recently, we and others observed that, in fact, greater BEC IFN-stimulated gene (ISG) expression in vivo (7) or in response to ex vivo viral infection (8) is associated with lower lung function in asthma donors. Furthermore, a recent case-control study of asthmatic children using nasal lavage samples prospectively through viral upper respiratory tract infections reported greater upregulation of ISG responses during viral illnesses that triggered acute exacerbations as compared with illnesses that did not, that this greater ISG expression associated with greater RV quantity and lower lung function throughout illness, and that lower pre-infection ISG expression associated with higher post-infection ISG expression and predicted higher risk

for exacerbation (9, 10). These results suggested that low baseline airway IFN tone in children with asthma may permit accelerated viral replication and exaggerated host responses underpinning increased exacerbation risk, but this hypothesis remained to be tested.

To directly test this hypothesis, we leveraged BEC organotypic cultures derived from well-characterized pediatric donors with and without asthma. While nasal samples are practical for clinical studies, they do not directly sample the lower airway, where asthma is manifest, and they represent mixtures of epithelial and immune cells characterizing a primary and secondary host response to virus. In contrast, BEC cultures represent the lower airway and are pure epithelial cells that retain key structural and functional features of the host's native airway epithelium, including mucociliary differentiation, innate immune signaling capacity, and donor-specific transcriptional programs. This model system enables precise temporal dissection of host-viral dynamics and allows for controlled perturbation of the pre-infection epithelial IFN milieu. By sampling from children with and without history of severe asthma exacerbations as well as healthy children without asthma, and experimentally modulating baseline IFN tone prior to RV infection, we aimed to determine whether low tonic IFN activity is a modifiable determinant of epithelial susceptibility to viral replication, downstream inflammatory responses, and exacerbation propensity. This approach offers a mechanistically grounded framework to identify epithelial immune phenotypes that predispose to exacerbation and may inform preventative or therapeutic strategies targeting epithelial antiviral readiness in children with asthma.

## Results

*Increased RV replication in BECs from children with severe asthma exacerbations.* Primary BECs were collected from children with asthma ( $n = 37$ ) and healthy children (HC;  $n = 3$ ). Among children with asthma, 23 had a history of severe exacerbation (SE), and 14 children had no severe exacerbation history (NSE) (Table 1). SE history was defined as history of exacerbation(s) requiring systemic corticosteroids and/or emergency department care/hospitalization for asthma (11). All 3 groups had similar ages, race, ethnicity, and body mass index. The 2 asthma groups had comparable fractional exhaled nitric oxide (FeNO) concentrations, spirometry values, total serum IgE concentrations, and allergen sensitization. At the time of BEC collection, a greater proportion of the SE group were taking inhaled corticosteroids.

Organotypic air-liquid interface BEC cultures (Figure 1A and Supplemental Figure 1; supplemental material available online with this article; <https://doi.org/10.1172/jci.insight.197711DS1>) were sampled before infection, infected with rhinovirus A16, and sampled at 2, 4, 7, and 10 days after infection. Differences in viral load levels and kinetics were compared over time among groups using both a linear model (LM) and a generalized additive mixed model (GAMM). BECs from SE donors demonstrated 5.9-fold higher viral copy number after infection compared with NSE donors (post-infection LM: Estimated Coefficient [Estimate] = 0.77,  $P = 2.2 \times 10^{-4}$ ; Figure 1B) with higher values throughout (GAMM Smooth Term [Shape],  $P = 2.0 \times 10^{-16}$ ). This result was also significant if the models were adjusted for use of inhaled corticosteroids or FeNO, neither of which showed a significant relationship with viral load.

*Children with severe exacerbations show sustained upregulation of inflammatory pathways and downregulation of metabolic pathways following RV infection.* Modular analysis of RNA sequencing (RNA-Seq) data from BEC samples among groups over the time series (day 0 to day 10) identified 19 of 42 differentially expressed modules comparing SE with NSE donors in a GAMM model (FDR < 0.05; Figure 1C and Supplemental Table 1). Of these, 11 of 19 modules also showed significant linear associations with viral load values across the post-infection time points (FDR < 0.05; Supplemental Table 2). We investigated the kinetic patterns and biological functions of these 11 modules and here highlight 5 modules of highest biological interest, with the remainder in Supplemental Table 3.

Three modules that were increased by RV infection and showed higher peak and/or greater sustained expression over time in the SE compared with NSE groups are shown in Figure 1, D–F. The first module is composed of 363 genes, predominantly canonical antiviral type I/III IFN response genes (annotated as “Interferon Response”; Supplemental Figure 2). BECs from SE donors exhibited a significantly higher average expression level at day 2, with a 1.69-fold increase compared with NSE donors (LM FDR =  $9.2 \times 10^{-3}$ ; Supplemental Table 4) and a 1.92-fold increase compared with HC with significantly different kinetics characterized by sustained higher levels at each post-infection time point among SE donors (SE vs. NSE GAMM Shape: FDR =  $3.5 \times 10^{-5}$ ; Figure 1D). This module was significantly associated with viral load (Estimate = 0.66; FDR =  $5.4 \times 10^{-20}$ ). It includes transcription factors involved in antiviral and inflammatory processes

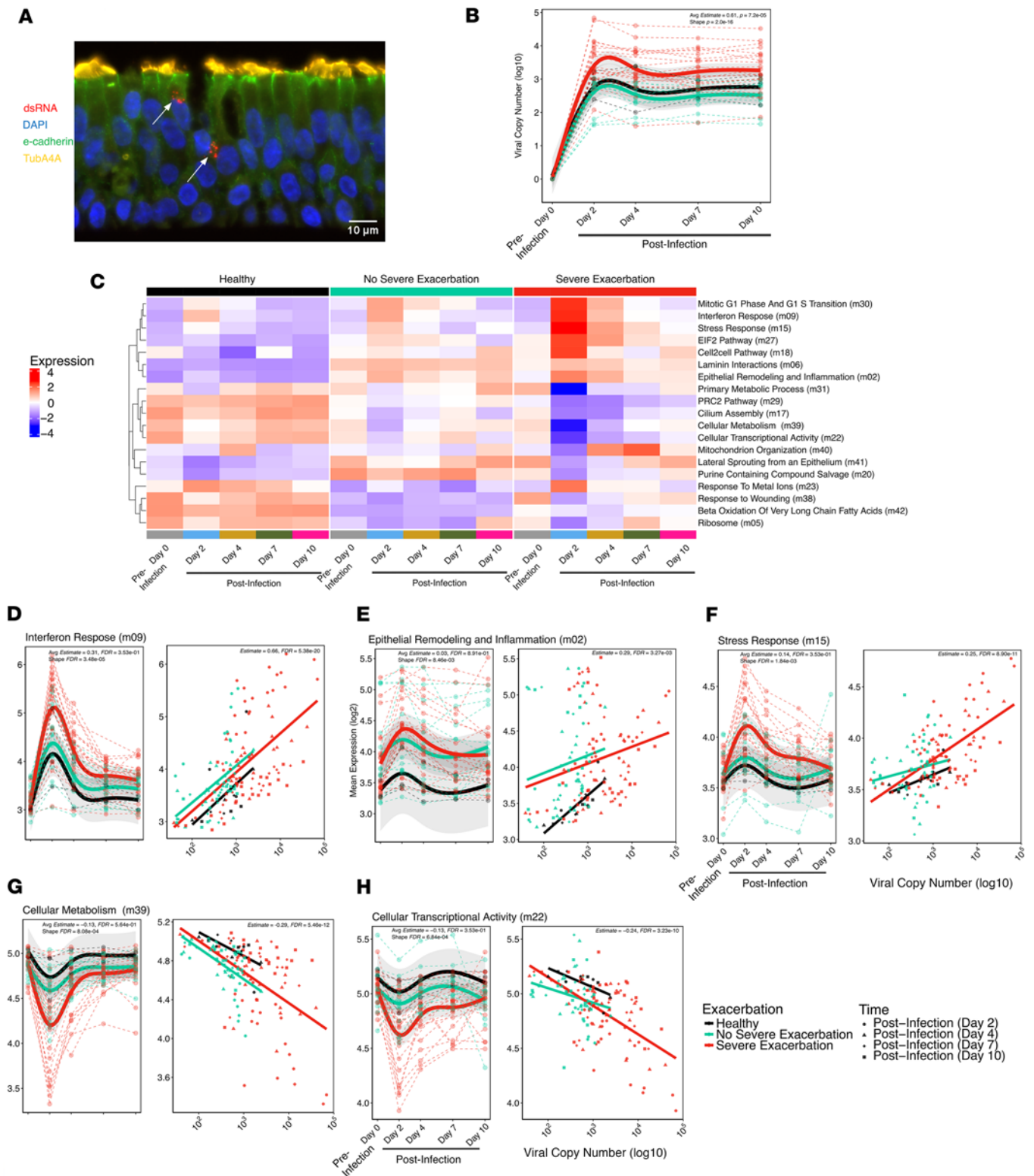


**Figure 1. BECs from children with severe asthma exacerbations show enhanced RV replication and sustained upregulation of IFN and inflammatory and dysregulated metabolic pathways.** (A) Immunofluorescence image of an asthma donor BEC culture 2 days after RV infection, stained with antibodies against e-cadherin (green), TubA4A (yellow), dsRNA (red). Nuclei stained with DAPI (blue). Arrows indicate replicating virus. Scale bar = 10  $\mu$ m. (B) GAMM plot showing viral load over time among clinical exacerbation groups and HC. (C) Heat map showing differentially expressed modules identified comparing the SE, NSE, and HC groups. Module expression levels shown as row normalized Z-scores of mean expression for each group and timepoint (columns) with red representing higher relative expression and blue representing lower relative expression. Module row ordering is by hierarchical clustering. The number in parentheses indicates the module number as defined by WGCNA. (D) Scatterplot showing the nonlinear changes in expression of the “Interferon Response” module over time by donor group. Linear regression plot showing association between the “Interferon Response” module and viral load

by donor group and time post infection (d2-10). (E) Analogous plots of the “Epithelial Remodeling and Inflammation” module demonstrating relationship between module expression and viral load. (F) Analogous plots of the “Stress Response” module demonstrating relationship between module expression and viral load. (G) Analogous plots of the “Cellular Metabolism” module demonstrating relationship between module expression and viral load. (H) Analogous plots of the “Cellular Transcriptional Activity” module demonstrating relationship between module expression and viral load. HC=15 samples from 3 donors, NSE=70 samples from 14 donors, SE=113 samples from 23 donors. Statistics indicate the SE vs NSE GAMM Shape FDR value, SE vs NSE GAMM Avg Estimate and FDR values and the all timepoint linear estimate and FDR values. Fit lines abased on a generalized additive mixed model including 95% confidence intervals.

(*IRF7*, *IRF1*, *STAT1*, *STAT2*), viral signaling molecules (*CXCL10*, *CXCL11*), and genes with RNA virus sensing properties (OAS family genes, *RIGI* and *IFIH1*). Interestingly, it also includes smaller subclusters of Th17 inflammation genes (e.g., *IL23A* and *IL12B*) and epithelial remodeling genes (*SMAD1*, *CCN4*, keratin and cytoskeleton genes).

A second module increased after infection in SE is composed of 1,396 genes with densely interconnected functions representing broad cellular functions including cell development and stimulus responses. Smaller subnetworks that are significantly enriched and of particular interest included TNF- $\alpha$  signaling, IL-17 signaling, and extracellular matrix organization. We annotated this module “Epithelial Remodeling and Inflammation.” Expression of this module similarly peaked at 2 days in all groups with non-significant 1.15-fold higher expression level at 2 days in SE versus NSE (LM FDR =  $6.5 \times 10^{-1}$ ) and 1.67-fold in SE versus HC but sustained significant elevation in SE at 4 days versus return to baseline levels in the NSE group (SE vs. NSE: GAMM Shape: FDR =  $8.5 \times 10^{-3}$ ; Figure 1E). Module expression was significantly associated with viral load (Estimate = 0.29, FDR =  $3.3 \times 10^{-3}$ ).

A third module increased in SE is annotated “Stress Response.” It includes 242 genes and is significantly enriched for unfolded protein and stress response genes (e.g., *VEGFA*, *NOD2*, *CEBPB*, *ATF4*), proteasome subunits, and steroid biosynthesis genes. This module was uniquely elevated in SE compared with NSE and HC across days 2–10 after infection. SE demonstrated 1.23-fold and 1.33-fold higher expression at 2 days compared with NSE (LM FDR =  $1.3 \times 10^{-2}$ ) and HC, respectively, and a sustained increase over time in SE (SE vs. NSE: GAMM Shape: FDR =  $1.8 \times 10^{-3}$ ; Figure 1F). Expression of this module was also significantly associated with viral load (Estimate = 0.25, FDR =  $8.9 \times 10^{-11}$ ).

Two modules that were decreased by RV infection and showed a lower nadir and lower sustained expression over time in SE compared with NSE and HC are shown (Figure 1, G and H). The first, which we annotated “Cellular Metabolism,” includes 106 genes and is significantly enriched for genes related to lipid oxidation, branched-chain amino acid degradation (e.g., *HADHB*, *MCCCI*, *ACADL*), and oxidative phosphorylation. Interestingly, this module also contains several genes related to  $\beta$ -adrenergic receptor signaling and muscarinic acetylcholine receptor signaling (*SNAP29*, *PRKX*, *ALDH6A1*). The nadir of expression of this module occurred at day 2, showing 1.30-fold and 1.52-fold lower expression in SE versus NSE (LM FDR =  $1.3 \times 10^{-2}$ ) and HC, respectively. This module remained lower in SE through the later time points (SE vs. NSE: GAMM Shape: FDR =  $8.1 \times 10^{-4}$ ). Expression of this module was inversely associated with viral load (Estimate =  $-0.29$ , FDR =  $5.5 \times 10^{-12}$ ).

The second such module includes 204 genes; the largest subset is relevant to cellular transcriptional activity, and a smaller subset is related to amino acid metabolism. We annotated this “Cellular Transcriptional Activity.” This module also nadired at day 2, showing 1.21-fold and 1.32-fold lower expression in SE versus NSE (LM FDR =  $1.28 \times 10^{-2}$ ) and HC, respectively, with expression remaining lower in SE asthma through day 10 (SE vs. NSE: GAMM Shape: FDR =  $6.8 \times 10^{-4}$ ). Expression of this module was also inversely associated with viral load (Estimate =  $-0.28$ , FDR =  $3.2 \times 10^{-11}$ ).

A linear model subset to the post-infection time points, days 2–10, was used to determine the extent to which observed viral load differences statistically mediated the observed differences in module expression between the SE and NSE groups for the 5 modules of interest. We observed that for the Interferon Response, Stress Response, Cellular Metabolism, and Cellular Transcriptional Activity modules, viral load mediated most of the difference in module expression observed between the 2 groups (Supplemental Figure 3 and Supplemental Table 5).

*Differences in pre-infection IFN tone relate to the observed greater viral replication in children with SE.* We investigated pre-infection differences in IFN tone between BEC cultures from SE and NSE that might explain the observed differences in viral infection kinetics. While there was no pre-infection difference in type I/III IFN gene expression between SE and NSE at a stringent FDR < 0.05, gene set enrichment analysis (GSEA) demonstrated lower aggregate expression of the hallmark IFN- $\alpha$  response pathway in SE compared with

NSE (Figure 2A). We measured protein concentrations of IFN- $\beta$ , IFN- $\lambda$ 2/IL-28A, IFN- $\lambda$ 3/IL-28B, and the IFN-stimulated chemokine CXCL10 in supernatant from BECs before infection and 2 days after RV infection. All 3 IFNs were below the assay detection limit in BECs before infection; IFN- $\beta$  remained below the assay detection limit in most samples following RV infection, while IFN- $\lambda$ 2 and IFN- $\lambda$ 3 were consistently detected following RV infection. In contrast, CXCL10 was readily detected with broad dynamic range in pre- and post-infection samples and was therefore used as a surrogate protein marker of IFN tone. We observed that pre-infection secreted CXCL10 protein concentrations were 3.32-fold lower in SE compared with NSE ( $P = 6.9 \times 10^{-4}$ ) and 2.88-fold lower compared with HC ( $P = 1.0 \times 10^{-1}$ ; Figure 2B, Supplemental Table 6, and Supplemental Figure 4). Furthermore, pre-infection BEC CXCL10 protein concentration was significantly associated with the subsequent post-infection viral load at day 2 in an inverse log-linear relationship (day 2; Pearson's  $R = -0.38$ ,  $P = 1.6 \times 10^{-2}$ ; Figure 2C and Supplemental Figure 5) and was also inversely associated with secreted IFN- $\lambda$ 2, IFN- $\lambda$ 3, and CXCL10 protein at day 2 following RV infection (Supplemental Figure 6 and Supplemental Figure 7).

*Prophylactic IFN- $\beta$  treatment reduces RV replication and ameliorates post-infection epithelial IFN, inflammatory, remodeling, and metabolism dysregulation.* To determine whether low IFN tone and/or low CXCL10 levels before infection are causal factors promoting RV replication and the differential post-infection inflammatory responses observed to be dysregulated in SE donors, we treated BEC cultures with IFN- $\beta$  or CXCL10 starting 2 days before RV infection and continuing for 2 days after RV infection. IFN- $\beta$  treatment led to a significant decrease in viral load at 2 days in comparison with the untreated samples in both asthma groups with a 4.22-fold decrease in the SE group ( $P = 4.81 \times 10^{-4}$ ) compared with a 3.39-fold decrease in the NSE group ( $P = 1.7 \times 10^{-4}$ ) (Figure 3A). Treatment of BEC cultures with CXCL10 did not impact viral load (data not shown). IFN- $\beta$  treatment also resulted in a 1.53-fold relative decrease in expression of the Interferon Response module at 2 days (Estimate =  $-0.61$ , FDR =  $1.2 \times 10^{-3}$ ; Figure 3B and Supplemental Table 7). Regression analysis demonstrated that the 2-day viral load had direct association with the expression of this module ( $\beta = 0.51$ ,  $P = 3.1 \times 10^{-86}$ ; Supplemental Table 8), indicating that IFN- $\beta$  treatment resulted in lower viral load, which significantly and completely mediated the relatively diminished Interferon Response module expression (Supplemental Table 9).

The Epithelial Remodeling and Inflammation module showed a 1.20-fold relative decrease in expression following IFN- $\beta$  treatment (Estimate =  $-0.27$ , FDR =  $2.2 \times 10^{-3}$ ), with significant positive association with viral load ( $\beta = 0.12$ , FDR =  $8.2 \times 10^{-19}$ ; Figure 3C), which also showed significant mediation. The Stress Response module exhibited a 1.14-fold relative decrease in expression with IFN- $\beta$  treatment (Estimate =  $-0.19$ , FDR =  $4.6 \times 10^{-3}$ ) and significant association with viral load ( $\beta = 0.10$ , FDR =  $6.6 \times 10^{-19}$ ; Figure 3D) and significant mediation. In contrast, CXCL10 treatment did not impact expression of the Interferon Response, Epithelial Remodeling and Inflammation, or Stress Response module (Supplemental Figure 8).

IFN- $\beta$  treatment also led to a relative restoration in expression levels of modules that had been significantly decreased in SE donors following infection. The Cellular Metabolism module displayed a 1.12-fold relative increase in expression with IFN- $\beta$  treatment (Estimate =  $0.16$ , FDR =  $4.2 \times 10^{-2}$ ) and an inverse relationship with viral load ( $\beta = -0.13$ , FDR =  $4.6 \times 10^{-25}$ ; Figure 3E) and significant mediation. Similarly, the Cellular Transcriptional Activity module showed a 1.09-fold relative increase in expression (Estimate =  $0.13$ , FDR =  $2.1 \times 10^{-2}$ ), an inverse association with viral load ( $\beta = -0.09$ , FDR =  $3.4 \times 10^{-24}$ ; Figure 3F), and significant mediation. CXCL10 treatment did not impact expression of either module.

*Single-cell RNA-Seq confirms and demonstrates the cellular sources of dysregulated responses to RV in children with SE.* To investigate epithelial cell type-specific responses in BECs before and after RV infection, we generated single-cell RNA-Seq data from a subset of donors in an independent experiment: SE ( $n = 7$ ), NSE ( $n = 4$ ), and healthy ( $n = 3$ ). These yielded 316,712 individual cells after filtering and quality control. Unsupervised, graph-based clustering identified 12 coarse cell clusters, which we annotated using cell type-specific markers for airway epithelial cells (12–14) (Figure 4A). This analysis revealed expected major epithelial cell populations as well as a unique population with the highest pre- and post-RV expression of a diverse array of inflammatory genes such as *ISG20*, *IFIH1*, *IFIT1*, *CXCL1*, *CXCL3*, *CXCL5*, *CXCL8*, and *CXCL10* (Figure 4B and Supplemental Table 10), alongside expression of markers typical of suprabasal, secretory, and goblet cells, consistent with a secretory lineage. We interpret these to be secretory-lineage cells involved in coordinating and/or propagating an innate immune response, consistent with some past observations (15), and label them secretory immune response cells (SIRs). We further mapped our cluster labels to the Human Lung Cell Atlas (HLCA), and all clusters corresponded to expected HLCA labels. Specifically, the

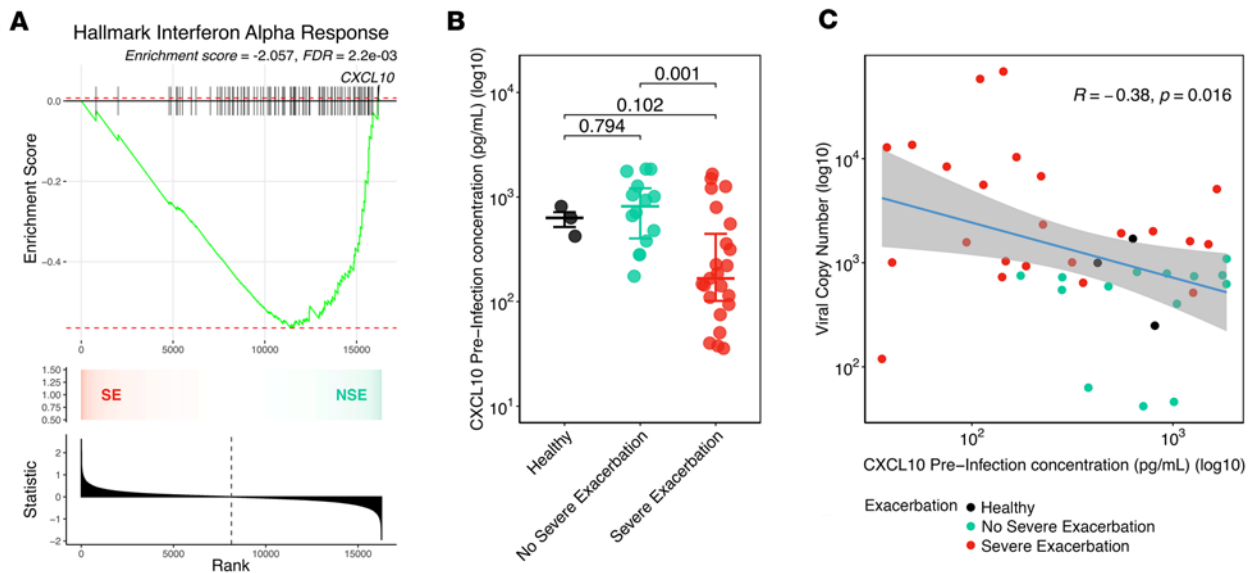


**Figure 2. Pre-infection IFN tone drives viral replication in children with SE.** (A) GSEA analysis shows a significantly negative enrichment score of the MSigDB hallmark IFN- $\alpha$  response gene set in the SE group compared with the NSE group in the pre-infection day 0 samples (GSEA enrichment score =  $-2.057$ ,  $FDR = 2.2 \times 10^{-3}$ ). The plot shows the running enrichment score for the gene set from decreasing values of the differential expression rank list. The peak represents the enrichment score for the gene set. The bars show the genes in the gene set ranked by effect size relative to all genes that are shown in the ranked list metric plot. The CXCL10 gene is indicated. The color gradient indicates which comparison group the genes appear in within the ranked list of genes. The bar plot at the bottom represents the effect size of all gene ranking. (B) Dot plot showing log-transformed pre-infection CXCL10 concentration values by exacerbation status; bars indicate median and interquartile range for each group. (C) Scatterplot showing a significant inverse relationship between log-transformed pre-infection CXCL10 values and log-transformed viral load at day 2 (Pearson's  $R = -0.38$ ,  $P = 1.6 \times 10^{-2}$ ). The fit line is based on a linear model including 95% CIs. HC,  $n = 3$  donors; NSE,  $n = 14$  donors; SE,  $n = 23$  donors.

SIR cell cluster mapped primarily to secretory cells (56%) and to a lesser extent to basal cells (31%), which is consistent with the HLCA not having a precise label for this mixed secretory/immune phenotype (Supplemental Figure 9). We identified these 12 cell populations in each sample/donor without any sample bias (Figure 4C and Supplemental Table 11); there were no significant differences in cell composition among donor groups (SE, NSE, and HC) or by pre- and post-infection status (Supplemental Figure 10). Custom viral probes were generated for the experiment and confirmed infection but showed relatively low hybridization, preventing statistically robust assessment of viral quantity at the single-cell level (see Methods and Supplemental Figure 11).

We investigated cell-level expression differences among donor groups in post-infection samples for the same modules derived from the bulk RNA-Seq analysis. We used ordinal regression to identify those modules with either a significant ascending (SE > NSE > HC) or descending expression trend (SE < NSE < HC) among donor groups (Supplemental Table 12). In the post-infection samples, the Interferon Response module was highest in SE asthma, showing an ascending trend in all but one cell type (Figure 4D and Supplemental Figure 12), consistent with the bulk transcriptomics data. The magnitude of this ascending difference among donor groups varied among cell types. Curiously, this module showed no expression difference among groups in the SIRs ( $FDR > 0.05$ ), which showed the highest overall expression of this module. Goblet cells showed relatively modest differences among groups (Estimate = 1.7,  $FDR = 4.7 \times 10^{-120}$ ). All other cell types showed fairly consistent large differences (Estimates = 3.0–4.9,  $FDR < 10 \times 10^{-10}$ ). Expression of this module was markedly increased in post-infection compared with pre-infection samples in all cell types and donor groups.

Expression of the Epithelial Remodeling and Inflammation module also showed an ascending trend in post-infection samples in all cell types. Magnitude varied markedly by cell type (Estimates = 1.1–13.9). This module expression difference by group was particularly pronounced in the tuft/pulmonary neuroendocrine cells (PNECs) (Estimate = 13.9,  $FDR < 10 \times 10^{-10}$ ) and SIRs (Estimate = 11.6,  $FDR < 10 \times 10^{-10}$ ). It was low in deuterosomal cells (Estimate = 1.1,  $FDR = 1.6 \times 10^{-2}$ ). The Stress Response module showed an ascending trend in post-infection samples (Estimates = 1.2–6.1). This was particularly pronounced in tuft/PNECs (Estimate = 6.1,  $FDR = 4.9 \times 10^{-10}$ ), ciliated cells (Estimate = 5.5,  $FDR < 10 \times 10^{-10}$ ), and

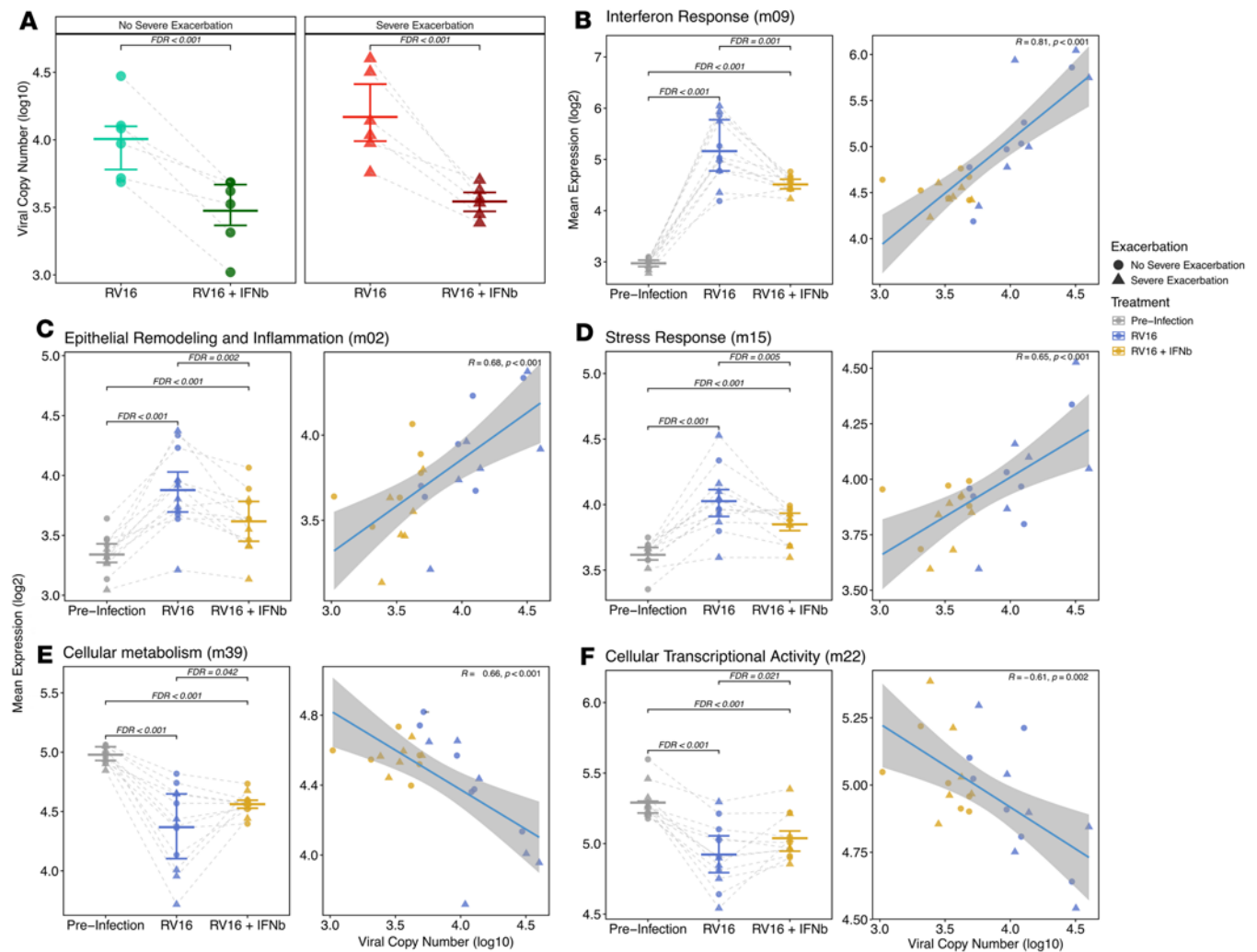


**Figure 3. Prophylactic IFN-β treatment reduces RV replication and ameliorates epithelial IFN, inflammatory, and remodeling pathways.** (A) Dot plot showing log-transformed viral copy number values by exacerbation status between samples at day 2 treated with IFN-β. The IFN-β-treated group showed a significant decrease in viral load compared with the untreated samples in both exacerbation groups with a 3.39-fold decrease in the NSE group ( $n = 6$  donors) and a 4.22-fold decrease in the SE group ( $n = 6$  donors); bars indicate mean and interquartile range for each group. (B) Dot plot showing expression changes in the Interferon Response module by IFN-β treatment. Regression plot showing association between the Interferon Response module and viral load by IFN-β treatment. (C) Dot plot showing expression changes in the Epithelial Remodeling and Inflammation module by IFN-β treatment. Regression plot showing association between the Epithelial Remodeling and Inflammation module and viral load by IFN-β treatment. (D) Dot plot showing expression changes in the Stress Response module by IFN-β treatment. Regression plot showing association between the Stress Response module and viral load by IFN-β treatment. (E) Dot plot showing expression changes in the Cellular Metabolism module by IFN-β treatment. Regression plot showing association between the Cellular Metabolism module and viral load by IFN-β treatment. (F) Dot plot showing expression changes in the Cellular Transcriptional Activity module by IFN-β treatment. Regression plot showing association between the Cellular Transcriptional Activity module and viral load by IFN-β treatment. Bars indicate median and interquartile range for each group, and the fit line is based on a linear model including 95% CIs.

SIRs (Estimate = 5.2, FDR <  $10 \times 10^{-10}$ ) but low in goblet cells (Estimate = 1.2, FDR =  $1.3 \times 10^{-9}$ ) and not significant in secretory cells.

The Cellular Metabolism and Cellular Transcriptional Activity modules showed descending expression trends (SE < NSE < HC) in post-infection samples consistent with the bulk transcriptomics data. Both modules showed similar trends among cell types, with differences particularly pronounced in tuft/PNECs and basal cells (Estimates = -7.4 to -13.9, FDR <  $10 \times 10^{-10}$ ) and least in deuterosomal cells (Estimates = -2.5 to -4.7, FDR <  $10 \times 10^{-10}$ ).

Further analysis of gene-level expression differences among the 3 donor groups was performed to identify additional cell-specific signals that might not have been detected in the module-level bulk transcriptomics data. In the post-infection samples, 5,160 unique genes showed an ascending trend among donor groups in one or more cell types, while 5,659 unique genes had a descending trend (Figure 5A and Supplemental

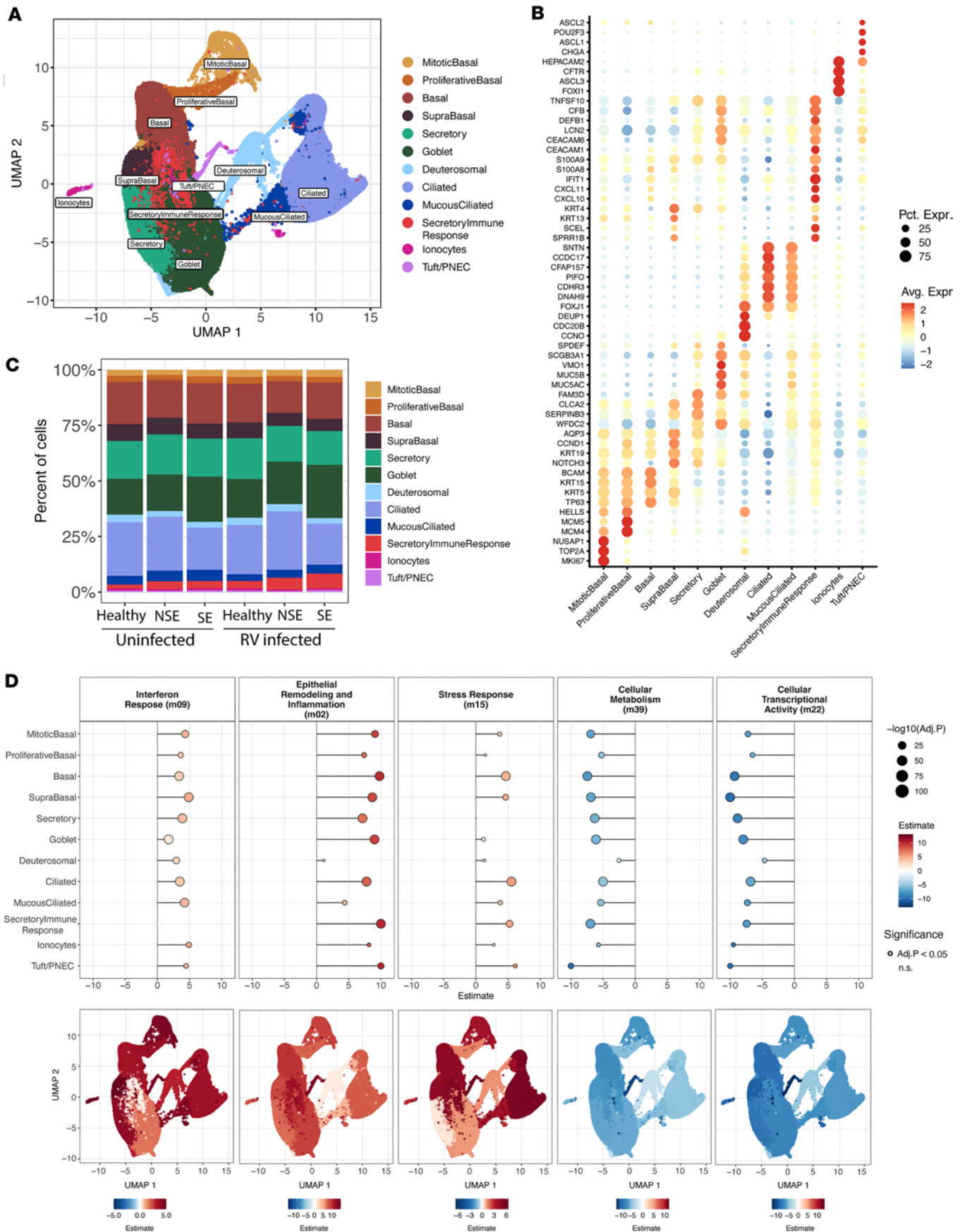


**Figure 4. Single-cell RNA-Seq maps epithelial cell diversity and reveals cell type-specific activation of bulk-derived transcriptional modules following RV infection.** (A) UMAP representation of the 316,712 cells recovered from samples collected from children with asthma (SE, 7 donors; NSE, 4 donors) and healthy controls ( $n = 3$  donors). Mitotic basal, 8,281 cells; proliferative basal, 8,405 cells; basal, 53,663 cells; suprabasal, 20,403 cells; secretory, 52,727 cells; goblet, 63,542 cells; inflammatory, 14,361 cells; deuterosomal, 8,836 cells; mucociliated, 13,284 cells; ciliated, 67,654 cells; ionocytes, 2,407 cells; tuft/PNECs, 2,251 cells. (B) The dot plot shows the expression of marker genes distinguishing distinct cell populations from the EmptyDrops-based processing pipeline (53). The color intensity indicates the magnitude of marker gene expression, and the size of the circle denotes percentage of cells expressing the marker gene. (C) Bar plot showing the mean proportions of identified epithelial cell populations by single-cell RNA-Seq by condition (uninfected samples and samples 2 days post-infection) and donor groups (SE, 7 donors; NSE, 4 donors; HC, 3 donors). (D) Dot plot showing the cumulative link model (CLM) estimates for select modules in RV-infected samples across all 12 cell types. The corresponding bottom plots show the relative CLM estimates on a UMAP space.

Table 13). The SIR cell cluster had the greatest transcriptional difference among donor groups (4,779 genes ascending, 488 descending). Genes with an ascending trend in the SIR cell cluster were a broad array of inflammatory molecules such as *IL1B*, *CXCL5*, *LCN2*, *FNI*, *LAMA4*, *CLIC5*, *GATA3*, and *ALOX5* (Figure 5B). The gene list was enriched for pathways related to lysosomes, focal adhesion, neutrophil extracellular trap formation, and antimicrobial response pathways.

To globally characterize the differences among donor groups by cell type in this gene level analysis, we performed pathway enrichment of the ascending and descending genes. Multiple immune, stress, and remodeling pathways, such as IFN responses, IL-6/JAK/STAT3 signaling, IL-17 signaling, TNF- $\alpha$ , and hypoxia, were enriched among those ascending genes highest in SE, particularly in SIRs, basal cells, tuft/PNECs, and goblet cells (Figure 5C and Supplemental Table 14). The asthma-associated pan-epithelial remodeling of IL-13 gene signature described by Jackson et al. was particularly enriched among ascending genes in goblet and basal cell populations (16). The asthma-associated inflammasome gene signature described by Radzikowska et al. was particularly enriched among ascending genes in SIRs and basal cell clusters (17). Among descending genes, lowest in SE, cilium assembly and related pathways were particularly enriched in ciliated and mucociliated cells, while transcriptional regulation and energy metabolism pathways were particularly enriched in secretory cells (Figure 5D and Supplemental Table 14). We also identified a “core gene signature” with consistent trend (same directionality and significance) and shared across 5 major cell populations, basal, secretory, goblet, ciliated, and SIR cells. This included 84 genes showing an ascending trend across donor groups (SE > NSE > HC) inclusive of viral response genes *RSAD2*, *ISG15*, *IFI30*, *IFIT2*, *OAS1*, *STAT1*, and *ZBP1*, chemokines and inflammation markers *CXCL6*, *CXCL8*, *CXCL10*, and *IL32*, and complement-related genes *C3*, *CFI*, *APOL1*, and *APOL2* (Figure 6). It included 48 genes with a descending trend across donor groups (SE < NSE < HC), including epithelial barrier function genes (*UPK1B*, *EPPK1*, *EVPL*) and antioxidant response genes (*GCLC*, *SELENOP*) (Supplemental Figure 13).

## Discussion

We have investigated kinetics of RV replication and host responses in organotypic bronchial epithelial cultures from well-characterized asthmatic and healthy children using bulk and single-cell RNA-Seq and targeted protein assessment. We found higher viral loads in cultures from asthmatic children with a history of severe exacerbations compared with those without or healthy controls. Transcriptomic modular analysis showed heightened and prolonged expression in SE donors of IFN response genes, inflammatory and remodeling pathways, and unfolded protein stress responses, all of which positively correlated with viral load. The Interferon Response module included not only canonical ISGs but also genes involved in Th17 inflammation and epithelial remodeling, which, together with the Epithelial Remodeling and Inflammation module, illustrate how impaired antiviral control may converge on broader proinflammatory and tissue-altering pathways in exacerbation-prone epithelium. In contrast, pathways related to cellular metabolism and transcriptional activity were downregulated in SE and inversely correlated with viral load. This cascade was evident in both bulk and single-cell analyses, with viral load statistically mediating the magnitude of these transcriptional responses and the differences observed in SE donors. Single-cell RNA-Seq further revealed how several epithelial subtypes contributed differentially to these amplified responses, with basal cells, secretory immune response cells, and tuft/PNECs showing particularly exaggerated post-infection activity.

Pre-infection samples from SE donors showed modestly lower type I IFN gene expression and reduced CXCL10 protein levels, which were inversely associated with post-infection viral load in a log-linear manner. This indicates that subtle deficits in baseline epithelial IFN tone confer susceptibility to greater RV

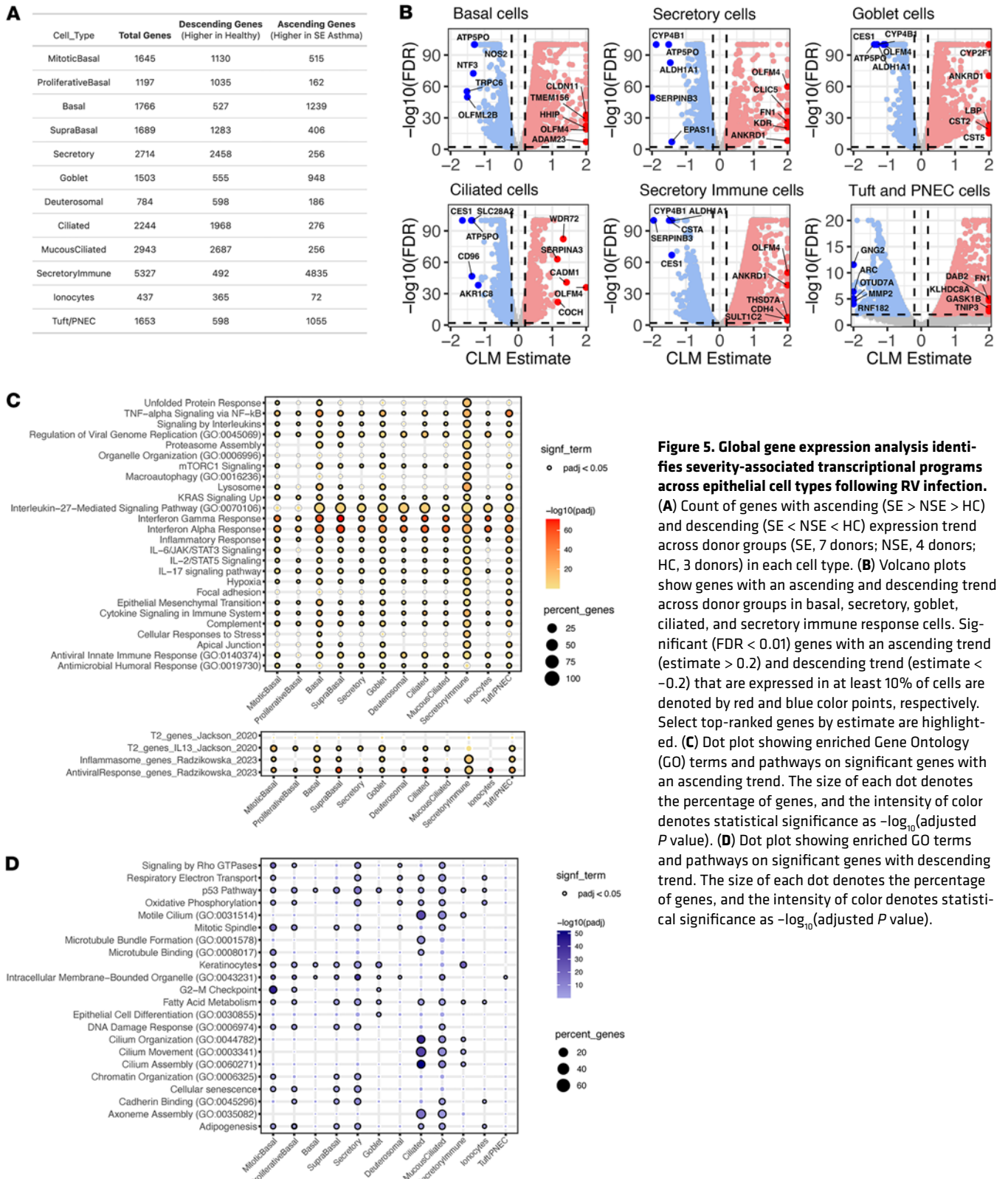


**Figure 5. Global gene expression analysis identifies severity-associated transcriptional programs across epithelial cell types following RV infection.** (A) Count of genes with ascending (SE > NSE > HC) and descending (SE < NSE < HC) expression trend across donor groups (SE, 7 donors; NSE, 4 donors; HC, 3 donors) in each cell type. (B) Volcano plots show genes with an ascending and descending trend across donor groups in basal, secretory, goblet, ciliated, and secretory immune response cells. Significant (FDR < 0.01) genes with an ascending trend (estimate > 0.2) and descending trend (estimate < -0.2) that are expressed in at least 10% of cells are denoted by red and blue color points, respectively. Select top-ranked genes by estimate are highlighted. (C) Dot plot showing enriched Gene Ontology (GO) terms and pathways on significant genes with an ascending trend. The size of each dot denotes the percentage of genes, and the intensity of color denotes statistical significance as  $-\log_{10}$ (adjusted *P* value). (D) Dot plot showing enriched GO terms and pathways on significant genes with a descending trend. The size of each dot denotes the percentage of genes, and the intensity of color denotes statistical significance as  $-\log_{10}$ (adjusted *P* value).

replication, and downstream dysregulation. To test causality, we treated cultures with IFN- $\beta$  before and during infection, which reduced viral replication and attenuated downstream transcriptional responses, including ISGs themselves. These findings prove how low baseline IFN tone can permit enhanced viral replication and resultant exaggerated inflammatory responses in airway epithelium from SE-prone children with asthma.

These findings provide mechanistic insight into how bronchial epithelial dysfunction can predispose children with asthma to severe exacerbations following RV infection. While prior studies have reported conflicting evidence regarding impaired versus exaggerated IFN responses in asthmatic epithelium (3–6, 18), our integrated approach helps reconcile these discrepancies. We show that children with a history of SE exhibit reduced basal IFN tone, which permits greater viral replication and, in turn, provokes amplified secondary IFN, inflammatory, stress, and remodeling responses. These findings refine our understanding of virus-triggered asthma exacerbations in children by demonstrating that deficient and exaggerated IFN responses can coexist in the same epithelium, but at distinct stages. While earlier studies emphasized impaired IFN responses in asthma (3, 4), more recent work, including that of Bhakta et al. and Altman et al., has linked excessive ISG expression to more severe disease and reduced lung function (7, 8). Our data reconcile these views, showing that children prone to exacerbation exhibit low baseline IFN tone that permits enhanced viral replication, which in turn drives an amplified secondary IFN, inflammatory, and remodeling response. This temporal duality helps explain prior conflicting findings and highlights the importance of assessing epithelial responses dynamically. Our results underscore and help explain recent clinical findings by Gaberino et al., which showed that lower pre-infection airway ISG expression predicted both higher risk of exacerbation and greater IFN upregulation during virus-triggered exacerbation events (10).

The broader upregulation of the Epithelial Remodeling and Inflammation and Stress Response modules in SE donors is notable. These modules included networks related to IL-17, TNF, and inflammasome signaling, all of which have been implicated in non-T2 or “neutrophilic” asthma endotypes (19–23). Although these pathways have often been studied in the context of pollutant exposure or bacterial infection (24–27), our findings indicate that RV alone can induce this proinflammatory, non-eosinophilic, airway remodeling milieu in SE epithelium, a finding recapitulated in the single-cell data. While biologics targeting IL-17 and TNF have failed to show benefit in unselected asthma populations (28, 29), perhaps only a subset of patients — e.g., those prone to severe RV-triggered exacerbations — may derive benefit from these treatment strategies. We also show that the unfolded protein response (UPR) and endoplasmic reticulum (ER) stress pathways are disproportionately activated in asthmatic children with SE. This aligns with prior observations in human asthma and animal models implicating maladaptive UPR and ER stress in epithelial dysfunction, goblet cell metaplasia, and airway remodeling (30–33). As UPR signaling has been shown to promote mucus production and viral replication (34, 35), therapeutic targeting of ER stress pathways could represent an additional strategy to mitigate post-infection epithelial injury in asthma. Strikingly, our single-cell data show that these transcriptional programs are active across multiple epithelial cell types but are notably pronounced in several non-ciliated populations — such as secretory immune response cells, tuft/PNECs, and basal cells — highlighting the emerging recognition of the importance of these cells in airway biology from a rapidly growing body of airway single-cell research (15, 36). Their exaggerated activation in SE donors suggests that epithelial cell-intrinsic programs — not merely infiltrating immune cells — are central to the pathophysiology driving virus-triggered asthma exacerbations. This pattern may reflect underlying genetic and/or epigenetic influences and aligns with prior studies showing that asthma-associated genetic risk variants and epigenetic modifications are enriched in genes expressed by airway epithelial cells (37–39).

Finally, our observation that IFN- $\beta$  pretreatment suppressed viral load and normalized downstream transcriptional responses strongly suggests a causal role for low basal IFN tone in predisposing to RV-induced exacerbations and epithelial dysfunction. While prior clinical trials of inhaled IFN- $\beta$  in unselected asthma populations and initiated after symptom onset showed limited efficacy (40), our data argue for a prophylactic strategy targeted toward individuals with documented low IFN tone, administered early in the course of infection or during high-risk seasons. Such a precision-based approach, guided by baseline epithelial immune profiling, could improve clinical outcomes with an already existing and safe potential therapeutic while reducing unnecessary treatment exposure.

Together, our results offer a comprehensive model in which deficient pre-infection IFN signaling in asthmatic bronchial epithelium permits RV replication, triggering exaggerated inflammatory, remodeling, and stress responses that contribute to the risk and severity of exacerbation. Our model integrates bulk and single-cell transcriptomic data and protein assessment, aligns with prior mechanistic and clinical observations, and identifies what we believe to be novel epithelial cell populations and pathways as potential therapeutic targets. In doing so, it refines current paradigms of RV-triggered asthma exacerbations by linking impaired basal antiviral tone with subsequent epithelial remodeling and proinflammatory cascades, a

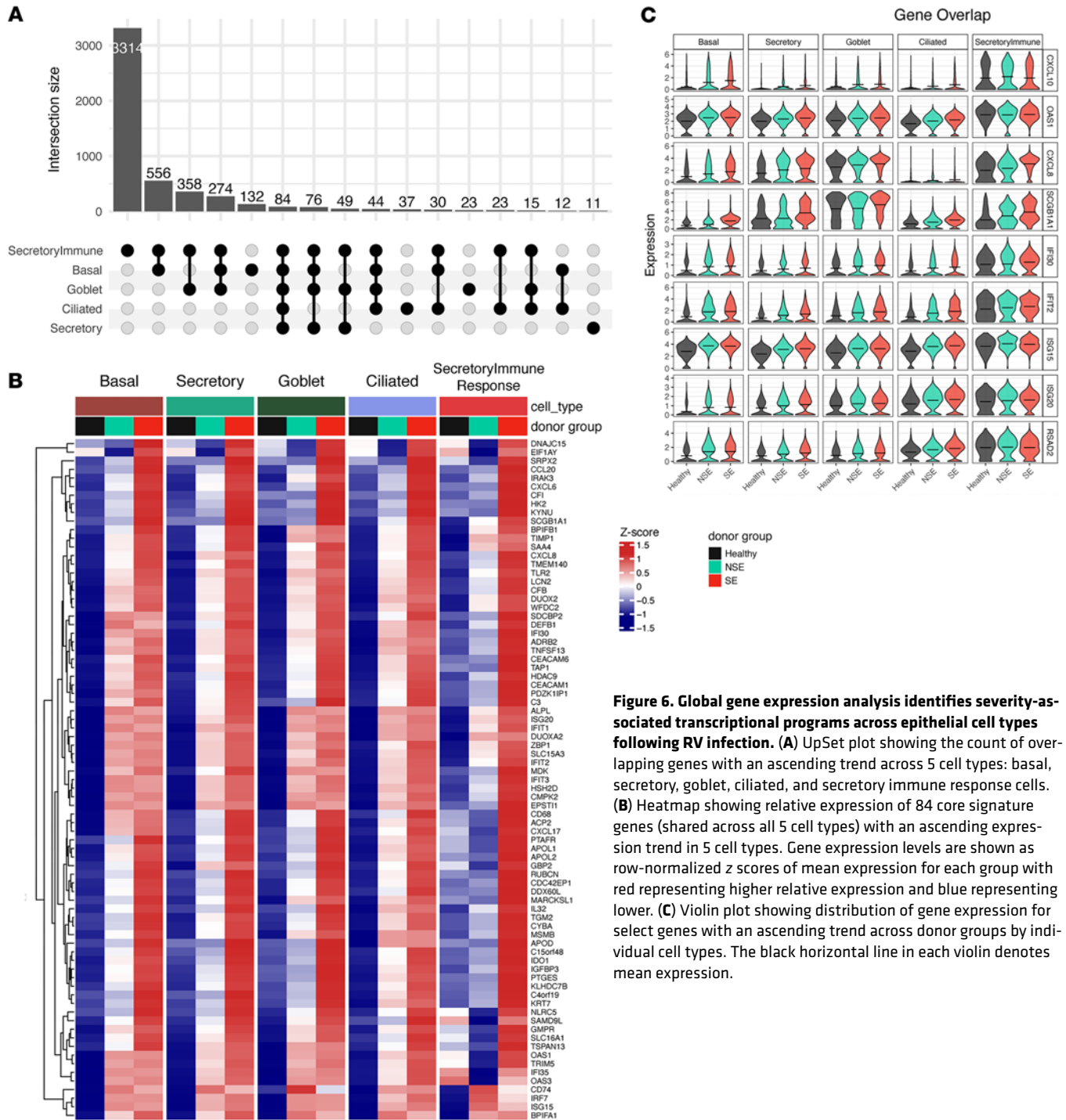


**Figure 6. Global gene expression analysis identifies severity-associated transcriptional programs across epithelial cell types following RV infection. (A)** UpSet plot showing the count of overlapping genes with an ascending trend across 5 cell types: basal, secretory, goblet, ciliated, and secretory immune response cells. **(B)** Heatmap showing relative expression of 84 core signature genes (shared across all 5 cell types) with an ascending expression trend in 5 cell types. Gene expression levels are shown as row-normalized z scores of mean expression for each group with red representing higher relative expression and blue representing lower. **(C)** Violin plot showing distribution of gene expression for select genes with an ascending trend across donor groups by individual cell types. The black horizontal line in each violin denotes mean expression.

connection only incompletely captured in prior studies. Future studies exploring the genetic and epigenetic underpinnings of low IFN tone and evaluating prophylactic immunomodulatory strategies in at-risk children with asthma are warranted.

There are several limitations to our study. Our post-infection sampling began at 2 days and therefore lacked earlier time points that might provide increased temporal resolution of the observed inflammatory cascade; this was informed by prior work showing peak immune responses and viral replication 48–96 hours after infection in organotypic air-liquid interface (ALI) cultures (8), which was consistent with in vivo observations (10). We used viral RNA copy number as a practical, cost-effective, and reproducible measure of viral load instead of trying to quantify infective virions; this was due to both technical and cost limitations of

**Table 1. BEC donor characteristics**

	All asthma donors (n = 37)	Healthy donors (n = 3)	Asthma SE donors (n = 23)	Asthma NSE donors (n = 14)	P value <sup>A</sup> (asthma SE vs. NSE donors)
Age (yr, mean ± SD)	11.7 ± 4.0	12 ± 3.5	11.2 ± 4.0	12.4 ± 3.9	0.39
Female sex	15 (41%)	1 (33%)	7 (30%)	8 (57%)	0.17
Male sex	22 (59%)	2 (66%)	16 (70%)	6 (43%)	
White	29 (78%)	3 (100%)	19 (83%)	10 (71%)	0.44
Black	5 (14%)	0 (0%)	3 (13%)	2 (14%)	1.0
Asian	2 (5%)	0 (0%)	1 (4%)	1 (7%)	1.0
American Indian or Alaska Native	1 (3%)	0 (0%)	0 (0%)	1 (7%)	0.38
Hispanic or Latino	6 (16%)	0 (0%)	4 (17%)	2 (14%)	1.0
Serum IgE (median [IQR])	103 [29.5, 220.5]	16 [15, 62]	115 [43, 237]	67.5 [9.8, 274]	0.31
≥2 Aeroallergen positive by allergen-specific IgE	19 (51%)	0 (0%)	11 (48%)	8 (57%)	0.74
FeNO (ppb; median [IQR])	10 [7, 18]	8 [5, 22]	11 [7, 23]	10 [7.5, 13]	0.33
Peripheral eosinophil count (cells/μL; median [IQR])	190 [129, 434]	55 [45, 122]	151 [126, 497]	199 [169, 397]	0.60
FEV <sub>1</sub> % predicted (yr, mean ± SD)	101.1 ± 14.6	114.6 ± 1.2	102.4 ± 12.7	98.5 ± 17.5	0.44
FEV <sub>1</sub> /FVC (yr, mean ± SD)	0.83 ± 0.06	0.84 ± 0.04	0.82 ± 0.07	0.84 ± 0.05	0.72
Inhaled corticosteroid use at time of BEC collection	16 (43%)	NA	12 (52%)	4 (29%)	0.19
LABA use at time of BEC collection	6 (16%)	NA	3 (13%)	3 (21%)	0.65
LTRA use at time of BEC collection	6 (16%)	NA	2 (8%)	4 (29%)	0.17
History of severe asthma exacerbation	23 (62%)	NA	23 (100%)	0 (0%)	<0.01
Body mass index (mean ± SD)	24.7 ± 8.2	21.8 ± 3.8	23.7 ± 8.5	26.5 ± 7.5	0.29
Atopic dermatitis	22 (60%)	NA	14 (61%)	8 (57%)	1.0
Allergic rhinitis	30 (81%)	NA	19 (83%)	11(79%)	1.0
Food allergy	9 (24%)	NA	5 (22%)	4 (29%)	0.70
History of allergy immunotherapy	5 (14%)	NA	4 (17%)	1 (7%)	0.63
Siblings	29 (78%)	2 (67%)	18 (78%)	11 (79%)	1.0
Cat or dog in the home	27 (73%)	2 (67%)	18 (78%)	9 (64%)	0.45
Environmental tobacco smoke exposure	4 (11%)	1 (33%)	2 (9%)	2 (14%)	0.62

<sup>A</sup>Welch's 2-tailed *t* test was used for normally distributed data, Mann-Whitney test for non-normally distributed data, and Fisher's exact test for contingency testing. BEC, bronchial epithelial cell; FeNO, fractional exhaled nitric oxide; FEV<sub>1</sub>, forced expiratory volume in 1 second; FVC, forced vital capacity; IgE, immunoglobulin E; IQR, interquartile range; LABA, long-acting β-adrenoceptor agonist; LTRA, leukotriene receptor antagonist; NSE, donors with no history of severe exacerbation; SE, donors with history of severe exacerbation.

conducting 50% tissue culture infectious dose (TCID<sub>50</sub>) or plaque assays from 248 unique ALI culture samples wherein accurate reproducible sampling from the apical surface would have been impaired by mucus layers of organotypic ALI cultures. Our small sample size of HC donors is a limitation, as larger numbers of donors would be needed to fully characterize the heterogeneity of transcriptomic responses to RV infection in healthy children. In this study, our design and statistical power were focused on the primary comparison between SE and NSE asthma groups, with HC included as a comparative reference point rather than for hypothesis testing. Assessing donor serum antibody levels against type I/III IFNs as well as rhinovirus A16 would provide valuable complementary information and would be an interesting future research direction that could help further elucidate mechanisms underlying differences between SE, NSE, and control groups. Unfortunately, these measurements were not performed in the current study, and we lack residual serum samples from subjects to measure serum antibody levels in this cohort. Although a highly unique strength

of our study is the ability to isolate bronchial epithelial responses in a robust sample size of carefully characterized children with and without asthma, the responses we observed reflect only epithelial responses lacking direct interaction with other immune cells that would be relevant in a clinical context. These findings suggest that disease-related epithelial programs are at least partly preserved in culture, underscoring both the utility and the limitations of ALI models and the need to integrate *in vivo* studies to fully capture epithelial response heterogeneity in asthma. RNA analysis of primary cells obtained at the time of brushing could provide valuable complementary information by linking the *in vivo* epithelial state to the transcriptional and epigenetic programs maintained in culture. Although not performed here, such paired analyses represent an important future direction to determine which signatures observed in ALI cultures most closely mirror transcriptional memory from the original epithelial progenitors.

In conclusion, bronchial epithelial cultures from asthmatic children with a history of severe exacerbations exhibited greater RV replication and exaggerated IFN, inflammatory, remodeling, and stress responses, alongside reduced metabolic and transcriptional activity, compared with those from NSE and healthy donors. These differences were strongly associated with lower pre-infection IFN-stimulated gene expression and CXCL10 protein levels. Prophylactic IFN- $\beta$  treatment reduced viral replication and normalized downstream responses, supporting low baseline IFN tone as a causal factor in viral susceptibility and epithelial dysregulation. These findings highlight resting epithelial IFN tone as a key determinant of host response heterogeneity and suggest that early, targeted immunomodulatory interventions may help prevent severe virus-induced exacerbations in susceptible children (40, 41).

## Methods

*Sex as a biological variable.* Both male and female participants were included in this study. Sex was recorded at the time of enrollment and included as a covariate in all relevant statistical analyses. Where appropriate, analyses were stratified by sex to examine potential sex-specific effects. No sex-based exclusion criteria were applied, and all procedures were performed uniformly across sexes.

*Study population and air-liquid interface cultures of bronchial epithelial cells.* Bronchial epithelial cells (BECs) from children with asthma ( $n = 37$ ) and HC ( $n = 3$ ) ages 6–18 years of age were obtained from subjects while under general anesthesia for an elective surgery using 4 mm Harrell unsheathed bronchoscope cytology brushes (ConMed) inserted through an endotracheal tube as we have previously described (8, 42). Cells were then seeded onto T-25 cell culture flasks (Corning) precoated with type I collagen and proliferated under submerged culture conditions using PneumaCult EX-Plus medium (Stemcell) (8). BECs (passage 2 or 3) were proliferated on Transwells under submerged culture conditions using PneumaCult EX-Plus medium (Stemcell) for 4–7 days, then differentiated to an organotypic pseudostratified ciliated state (Supplemental Figure 1) for 21 days at ALI using PneumaCult ALI medium (Stemcell) as previously described (8, 43–45). We have previously demonstrated stability of gene expression in primary BEC ALI cultures between passages 1 and 3 (46).

*Clinical characterization of BEC donors.* BEC donors were carefully clinically characterized. Blood was drawn for total serum IgE, eosinophil count, and allergen-specific IgE against common aeroallergens (cat, dog, *Dermatophagoides farinae*, *D. pteronyssinus*, *Alternaria tenuis*, *Aspergillus fumigatus*, and timothy grass). Subjects completed a clinical phenotyping visit that included (a) a detailed review of medical and social history (e.g., asthma exacerbation history, medication use, environmental tobacco smoke exposure, cat and dog exposure, siblings in home), (b) review of atopy history (past skin prick test or allergen-specific IgE testing, physician-treated atopic dermatitis, allergic rhinitis, and food allergy, treatment, and history of allergy immunotherapy), (c) measurement of total IgE and an aeroallergen-specific IgE panel, (d) performance of spirometry, and (e) measurement of fractional exhaled nitric oxide (FeNO). Spirometry was performed in accordance with American Thoracic Society/European Respiratory Society (ATS/ERS) standards and recommendations (47), and percentage predicted spirometric parameters was calculated using Global Lung Function Initiative spirometry race-neutral reference equations (48). FeNO was measured in accordance with ATS guidelines (49). History of a severe asthma exacerbation was defined as an increase in asthma symptoms requiring (a) systemic corticosteroids for 3 or more consecutive days, or (b) hospitalization or emergency department visit for asthma symptoms (11).

*Human rhinovirus infection.* BEC cultures were infected on the apical surface with human rhinovirus A16 (RV-A16; ATCC) at a multiplicity of infection (MOI) of 0.5. Viral suspension was removed from the apical surface after 2 hours of incubation with no subsequent rinsing. Viral load was measured in BECs at 2, 4, 7, and 10 days after infection using Genesis Human Rhinovirus Subtype 16 PCR Kit (Primerdesign).

**Table 2. Custom rhinovirus probes for 10x Genomics Flex single cell RNA-seq**

LHS	RHS
5'-CCTTGGCACCCGAGAATTCAGTGGTGTGGGATGTAGGTTTACAAT-3'	/5Phos/-CTACAGTGCATTGGTTGTACCATGAAAAAAAAAAAAAAAAAAAA AAAAAAAAAAAAAAAA-3'
5'-CCTTGGCACCCGAGAATTCAGTGGTGTGGGATGTAGGTTTACAAT-3'	/5Phos/-GATTACATACACATGCTCGGTGAAGAAAAAAAAAAAAAAAAAAAA AAAAAAAAAAAAAAAA-3'
5'-CCTTGGCACCCGAGAATTCACATGGGAACTTTGTGTTCCGGTATT-3'	/5Phos/-GTGACCAGTGAGCAATTACACAAAGAAAAAAAAAAAAAAAAAAAA AAAAAAAAAAAAAAAA-3'
5'-CCTTGGCACCCGAGAATTCAGCCTACGCAAAGCCTAGTAATACAT-3'	/5Phos/-TGAAAGATACTGGTTGGTCCGCTCAAAAAAAAAAAAAAAAAAAAA AAAAAAAAAAAAAAAA-3'
5'-CCTTGGCACCCGAGAATTCACAAGAGGCGACTCAACCATAACAT-3'	/5Phos/-CTCAAGATGTTGCTAATGCAGTGGTAAAAAAAAAAAAAAAAAAAA AAAAAAAAAAAAAAAA-3'
5'-CCTTGGCACCCGAGAATTCAGCACTTCTGTTTCCCGGTCAAAGT-3'	/5Phos/-TGATATGCTCCACAAGGCAAAAACAAAAAAAAAAAAAAAAAAAA AAAAAAAAAAAAAAAA-3'

*Scanning electron microscopy.* Transwells were fixed in 2% paraformaldehyde and 2% glutaraldehyde in 0.1 M phosphate buffer at 4°C, then rinsed with 0.1 M phosphate and postfixed in 1% osmium tetroxide overnight at 4°C. Following three 10-minute washes with water, samples were gradually dehydrated to 100% EtOH at 10% increments. A biopsy punch tool was used to remove the Transwell membranes to be critical point dried. Samples were then gold sputter coated and imaged using a FEI Quanta 200F scanning electron microscope.

*Immunofluorescence microscopy.* AECs cultured in Transwells were fixed in 10% neutral-buffered formalin and washed in PBS before being embedded in paraffin. After sectioning and deparaffinization, samples were permeabilized with 0.3% Triton X-100 for 5 minutes, treated with 20 µg/mL proteinase K (Invitrogen catalog 25530049) for 6 minutes for antigen retrieval, and blocked with 10% normal goat serum (NGS; Vector Laboratories catalog S-1000-20) for 1 hour at room temperature. Sections were incubated with rabbit anti-E-cadherin (Cell Signaling Technology catalog 3195; 1:50) and mouse anti-tubulin A4A (Invitrogen catalog PA5-105102; 1:200) in staining buffer (PBS plus 1% NGS plus 0.1% Triton X-100) overnight at 4°C, washed 3 times in PBS-T (PBS with 0.1% Tween 20), and incubated with Alexa Fluor 488-conjugated goat anti-rabbit (Invitrogen catalog A32731; 1:1,000) and Alexa Fluor 594-conjugated donkey anti-mouse (Invitrogen catalog A-21203; 1:1,000) antibodies. After washing, sections were re-blocked in 10% NGS and incubated with mouse anti-dsRNA (SCICONS, clone J2; Absolute Biotech, used at 1:100) pre-conjugated to Alexa Fluor 647 with Zenon mouse IgG<sub>2a</sub> labeling kit according to the manufacturer's instructions (Invitrogen catalog Z25108). Stained sections were mounted with ProLong Gold with DAPI (Invitrogen catalog P36935) and allowed to cure overnight. Slides were then imaged on a Leica DM6000 widefield microscope, and images were processed using ImageJ (NIH).

*Protein analysis.* Protein concentrations of CXCL10, IFN-β, IFN-λ2/IL-28A, and IFN-λ3/IL-28B were measured in supernatant from uninfected BEC cultures and BEC cultures 2 days after RV infection via a Human Luminex Discovery Assay (R&D). IFN-β concentrations were found to be below the assay detection limit in all samples from uninfected BECs and in many samples after RV infection (data not shown). IFN-λ2 and IFN-λ3 were also below detection limits in many uninfected samples but were consistently detected after RV infection. For analyte concentrations above the assay detection limit in neat samples following RV infection, supernatant was assayed following a 10-fold dilution in Luminex assay diluent.

*RNA collection.* RNA was collected from BEC cultures before infection and at 2, 4, 7, and 10 days after RV infection. To collect RNA from BEC cultures, medium was first removed from the basolateral chamber of Transwells. Eight hundred microliters of lysis buffer (Invitrogen product AM1912) was added to the apical surface of cultures. A pipette tip was then used to gently scratch each apical well in a crosshatch pattern to loosen BECs from the Transwell membrane. RNA was extracted using the RNAqueous kit for total RNA isolation (Thermo Fisher Scientific).

*IFN-β and CXCL10 treatment experiments.* BEC cultures from SE (n = 6) and NSE (n = 6) donors were treated with IFN-β or CXCL10 starting 2 days before RV infection and continuing for 2 days after RV

infection. Recombinant human IFN- $\beta$  (1 ng/mL; Abcam) or CXCL10 (2 ng/mL; R&D Systems) was added to BEC ALI medium starting 2 days before RV infection and refreshed with each medium change (every other day). Two days after initiation of treatment with IFN- $\beta$  or CXCL10, BEC cultures were infected with human RV-A16 at an MOI of 0.5 as described above. RNA was collected from BEC cultures before infection and 2 days after RV infection.

*RNA-Seq and data processing.* Total RNA was used to construct libraries by using the SMART-Seq v4 Ultra Low Input RNA Kit for Sequencing (Takara), with reverse transcription followed by PCR amplification to generate full-length amplified cDNA. Sequencing libraries were constructed using the NexteraXT DNA sample preparation kit with unique dual indexes (Illumina) to generate Illumina-compatible barcoded libraries. Libraries were pooled and quantified using a Qubit Fluorometer (Thermo Fisher Scientific). Sequencing of pooled libraries was carried out on a NextSeq 2000 sequencer (Illumina) with paired-end 53-base reads with a target depth of 5 million reads per sample. Base calls were processed to FASTQs on BaseSpace (Illumina), and a base call quality-trimming step was applied to remove low-confidence base calls from the ends of reads. Resulting Bcl files were deconvoluted and converted to FASTQ format using Casava from Illumina. FASTQ files were aligned to the Ensembl version of the human genome (GRCh38, Ensembl 91) by STAR (version 2.4.2a). HTSeq-count (version 0.4.1; <https://htseq.readthedocs.io/>) was used to generate gene counts with mode as “intersection (nonempty)” and minimum alignment quality set to 20 and otherwise set to default parameters. Quality metrics were compiled from Picard (version 1.134; <https://broadinstitute.github.io/picard/>), FastQC (version 0.11.3; [www.bioinformatics.babraham.ac.uk](http://www.bioinformatics.babraham.ac.uk)), Samtools (version 1.2; [www.htslib.org](http://www.htslib.org)), and HTSeq-count (version 0.4.1). For quality control, samples that had human-aligned counts greater than 1 million mapped reads and a median coefficient of variation coverage less than 0.7 were kept. Genes were filtered to include those that had a trimmed mean of  $M$  value normalization count of at least 0.3 in at least 10% of samples, and further filtered for only protein-coding genes. Normalized counts were transformed to  $\log_2$  counts per million mapped reads along with observation-level weights using voom-WithQualityWeights from the limma R package (version 4.2.1). The final dataset for the time series analysis of SE versus NSE versus HC donors included 198 samples composed of 16,275 genes and, for the IFN- $\beta$  and CXCL10 conditioning experiments, 48 samples composed of 15,907 genes.

*Single-cell analysis sample preparation.* For single-cell RNA-Seq, BECs from a subset of the children with asthma ( $n = 11$ ) and HC ( $n = 3$ ) were differentiated ex vivo at ALI to generate organotypic cultures and infected with human RV-A16 at an MOI of 0.5 as described above. To dissociate differentiated BEC ALI cultures into a single-cell suspension, the apical surface of the Transwell was treated with 0.5 mL of 10 mM dithiothreitol (DTT; Thermo Fisher Scientific) in 1 $\times$  PBS (Gibco) for 10 minutes at 37°C to remove accumulated mucus, subsequently washed 3 times with 0.5 mL of 1 $\times$  PBS (Gibco) to remove excess DTT, and then treated with 300  $\mu$ L TrypLE Express (Gibco) warmed to 37°C, with 600  $\mu$ L TrypLE Express added to the basolateral chamber. Wells were incubated for 15 minutes at 37°C, then mechanically dissociated by pipetting 10 times with a P1000 pipette. The cell suspension was transferred into an empty 15 mL conical tube, where the cell suspension was further pipetted until visually homogeneous, and wells were rinsed with warm EX Plus medium (Stemcell). Cells were mixed by pipetting 20 times with a 5 mL serological pipette set to slow and then centrifuged at 250g for 7 minutes. The cell pellet was resuspended with 1 mL of 0.04% BSA (Invitrogen) in 1 $\times$  PBS and gently pipetted 30 times, and an additional 1 mL of 0.04% BSA in PBS was added. The cell suspension was then filtered twice through a 30  $\mu$ m cell strainer (pluriSelect, Life Science) and centrifuged at 150g for 10 minutes. The 10x Genomics Chromium Next GEM Single Cell Fixed RNA Sample Preparation Kit was used to fix the BECs. The cell pellet was resuspended in 1 mL of Fixation Buffer (10x Genomics), pipetted to mix 10 times, and stored overnight at 4°C. The fixed single cells were then centrifuged at 850g for 7 minutes, resuspended with 1 mL chilled Quenching Buffer (10x Genomics), and pipetted to mix 5 times on ice. The cell suspension was transferred to 2 mL lo-bind tubes (Eppendorf), 100  $\mu$ L Enhancer (10x Genomics) warmed to 65°C was added and mixed, and 265  $\mu$ L 50% glycerol was added and mixed into the fixed cells. Samples were stored at -80°C until further post-storage processing and sequencing.

Fixed samples were processed according to the manufacturer's instructions, using the Chromium Next GEM Single Cell Fixed RNA Sample Preparation Kit. Briefly, fixed samples were thawed and hybridized overnight to 1 of 4 human probe sets (10x Genomics), with or without additional spiked-in custom RV probes. Pooled samples were washed and loaded onto a Chromium X (10x Genomics) for partitioning into GEMs. Gene expression libraries were generated according to the Chromium Fixed RNA Profiling

Reagent Kits for Multiplexed Samples user guide. Sequencing was carried out on a NextSeq 2000 sequencer, using NextSeq 2000 P4 XLEAP-SBS flow cells (Illumina) with a target depth of 10,000 reads per cell.

Custom RV probes for 10x Genomics Flex were designed targeting the human RV-A16 genome (GenBank L24917.1). Following 10x Genomics specifications, probes consisted of 50 bp target sequences split into 25 bp left-hand side (LHS) and right-hand side (RHS) segments, with 44%–72% GC content, a T at the 3' end of the LHS, no homopolymer runs greater than 3, and minimal target site competition. Primer-BLAST (NCBI) was used to identify candidate sequences with human genome specificity (taxID: 9606). From 40 valid targets, 8 met all criteria including a 25th-position T; 3 were excluded due to binding overlap, leaving 5. Reverse-strand primers were reverse-complemented to generate RHS probes. Final sequences were manually verified for human genome specificity. A sixth validated probe was added based on extensive use in RV quantitative PCR work (50). Probe sequences are shown in Table 2.

*Single-cell RNA-Seq data processing and analysis.* Single-cell RNA-Seq 10x dataset pre-processing including cell demultiplexing and alignment was performed using Cell Ranger Single-Cell Software Suite (version 7.0.0, 10x Genomics). We used the human reference genome (GRCh38, Ensembl 91) for alignment and generated raw and filtered cell-by-gene-count matrix files.

The filtered cell-by-gene-count matrix file was used for the standard Cell Ranger-based data processing pipeline. First, we removed genes expressed in fewer than 4 cells. Next, we excluded cells with fewer than 100 genes detected or cells with more than 20% mitochondrial reads. Further, to eliminate possible doublet cells, we removed cells with more than 7,000 genes detected. The count data were then normalized to 10,000 reads per cell using the NormalizeData function. Samples were integrated using a stepwise canonical correlation analysis approach with the IntegrateLayers function on 20 dimensions and 2,000 variable genes. After integration, principal component analysis (PCA) was performed on the integrated data using the RunPCA function with the first 50 principal components. This was followed by uniform manifold approximation and projection (UMAP) using the RunUMAP function with 50 dimensions, and clustering was performed using the FindNeighbors and FindClusters functions with a resolution of 0.85 to identify distinct cell clusters. Cluster-specific markers for each cluster were identified using the FindAllMarkers function, and then cell clusters were manually annotated by assessment of the expression of cluster-specific markers to known cell type markers. Mitotic basal cells were annotated by the expression of cell cycle markers such as TOP2A, MKI67, and NUSAP1; proliferative basal cells were annotated by MCM4, MCM5, and HELLS; basal cells by the expression of TP63, KRT5, KRT15, and BCAM; and suprabasal cells by NOTCH3 and KRT19. We identified secretory cells by unique expression of SERPINB3 and CLCA2, and goblet cells by MUC5AC, MUC5B, and VMO1. We identified 3 cell clusters within ciliated cells: deuterosomal cells by CCNO, DEUP1, and CDC20B, ciliated cells by FOXJ1, PIFO, CDHR3, SNTN, and DNAH9, and mucociliated cells by expression of a combination of ciliated markers and lower levels of mucin genes such as MUC5AC and MUC5B. We also identified rare cell populations such as ionocytes by the expression of FOXI1, CFTR, and ASCL3, and tuft (brush) cells and PNECs by the expression of POU2F3, ASCL2 and CHGA, and ASCL1. Additionally, we observed a distinct cluster representing cells in an inflammatory state with the expression of genes such as ISG20, IFIH1, IFI30, IFIT1, IFIT2, IFIT3, and CXCL10. All the analyses were performed in the Seurat R package (version 5.0.1) (51).

*Statistics.* To compare viral load differences over time among the SE, NSE, and HC groups, a generalized additive mixed model (GAMM) was run with an interaction between time and group and a random effect for epithelial cell donorID. This was done using the R package mgcv with model syntax of  $\log_{10}(\text{viral load}) \sim \text{group} + \text{s}(\text{time}) + \text{s}(\text{time}, \text{by}=\text{group})$ . The differences in means across time, abbreviated throughout as the Average Difference (Avg), are presented, as are the differences in the smoothing terms among groups (Shape). Differences in viral load restricted to the 2-day time point were assessed using a linear model, and the differences in means (Estimate) are presented.

To compare baseline protein levels between SE, NSE, and HC, a linear model was used with model syntax of  $\log_{10}(\text{protein analyte concentration}) \sim \text{group}$ . Association between baseline BEC CXCL10 protein concentration and post-infection viral load was analyzed using a linear model with syntax:  $\log_{10}(\text{viral load}) \sim \log_{10}(\text{CXCL10 protein analyte concentration})$  with epithelial cell donorID as a random effect; cross-sectional association with day 2 viral load was analyzed using Pearson's correlation. GSEA was performed using the hallmark gene sets from the Molecular Signatures Database (MSigDB). Genes were ranked based on  $\log_2$  fold change for the 2 exacerbation groups (SE and NSE) at baseline. GSEA was performed using the fgsea package in R with 10,000 gene set permutations to assess statistical significance.

Normalized enrichment scores and adjusted  $P$  values were reported, and significant pathways were identified using a false discovery rate (FDR) cutoff of 0.2 or below by the Benjamini-Hochberg procedure.

Differentially expressed genes were identified using GAMMs comparing expression differences over time between the 2 exacerbation groups (SE and NSE) as an interaction term on the first half (99 of 198) of samples. The model syntax was  $\text{gene\_expression} \sim \text{exacerbation\_group} + \text{s(time)} + \text{s(time,by=exacerbation\_group)}$  including a random effect for epithelial cell donorID. This identified 6,714 genes that reached an FDR-adjusted  $P$  value less than 0.25 by the Benjamini-Hochberg procedure for any of the 3 fixed effect terms. These genes were then used for supervised weighted gene coexpression network analysis (WGCNA) to identify genes with similar expression patterns and group them into modules. The WGCNA parameters used were minimum module size of 20, maximum module size of 500, deep split of 3, and a soft threshold (power) of 10, which was selected as the lowest soft threshold resulting in a scale-free topology model fit  $R^2$  greater than 0.8. This resulted in 42 modules for downstream analysis. Module values were summarized by taking the mean of all genes ( $\log_2$  transformed values) in the respective module. Using the gene composition of each module, these modules were generated for all samples for all the downstream analysis. These modules were then modeled using the same GAMM syntax to identify those showing differential expression patterns over time among SE, NSE, and HC groups at a stringent FDR  $< 0.05$  for the interaction and/or group intercept terms. Multiple testing correction was performed using the Benjamini-Hochberg procedure. For each module that showed a significant difference among groups, pathway enrichment was performed using the clusterprofiler R package, which calculates a hypergeometric FDR-corrected  $P$  value for enrichment of public gene sets. We used the Gene Ontology biological processes (GO\_BP), Kyoto Encyclopedia of Genes and Genomes, Reactome, Biocarta, and MSigDB hallmark gene sets for enrichment. The 5 modules presented in the main text were annotated based on manual inspection of the enrichment terms and module genes. Linear mixed-effects models were used to identify modules significantly associated with viral load in the post-infection samples using the R package *kimma* (52). The model syntax was  $\text{module\_expression} \sim \log_{10}(\text{viral load}) + \text{time}$ , including a random effect for epithelial cell donorID. For the mediation analysis, 2 linear models were compared using only the post-infection samples. The syntax of the first model was  $\text{module\_expression} \sim \text{exacerbation} + \text{time}$  including a random effect for epithelial cell donorID to compare module expression between SE and NSE. The second model used the same syntax but with the addition of  $\log_{10}$ -transformed viral load as a covariate to regress out the effects of viral load. The effect size and  $P$  values for each module were then compared between the 2 models. The above models were also run adjusting for sex where the results were congruent.

To determine the effect of IFN- $\beta$  or CXCL10 on RV replication, viral load was quantified at 2 days after infection and compared across 3 treatment conditions using a linear mixed model with syntax:  $\log_{10}(\text{viral load}) \sim \text{Treatment}$  including a random effect for epithelial cell donorID separately for SE and NSE groups. A similar model was used to compare module expression across treatment conditions adjusted for median coefficient of variation coverage using the syntax:  $\text{module\_expression} \sim \text{Treatment} + \text{median\_cv\_coverage}$ , including a random effect for donorID.

*Study approval.* BECs from children were obtained and used in these experiments under studies 12490 and 1596 approved by the Seattle Children's Hospital Institutional Review Board. Parents of subjects provided written informed consent, and children over 7 years of age provided assent.

*Data availability.* All raw bulk and single-cell RNA-Seq data have been uploaded to the NCBI's Gene Expression Omnibus database (GEO GSE309705). Supporting data values associated with the main article and supplemental material (including values for all data points shown in graphs and values behind reported means/medians) are included as a single Supporting Data Values XLS file.

## Author contributions

JSD and MCA designed the studies. MPW recruited and enrolled human subjects. PCDC, LMR, ERV, CRG, NBS, KW, and JSD performed the experiments. NDJ, BB, PCDC, AJN, and MCA performed the RNA sequencing analysis. PCDC, BB, WTP, NDJ, MCA, and JSD wrote the manuscript. PCDC, BB, WTP, NDJ, LMR, NBS, KW, AJN, ERV, CRG, MPW, TSH, SFZ, MCA, and JSD edited the manuscript. All authors reviewed and approved the manuscript before submission. NDJ and BB are co-first authors. NDJ is listed first because they performed the single cell sequencing analysis and wrote the methods and interpretation of that data in the context of bulk RNA sequencing data. BB contributed key analyses of bulk RNA-sequencing and protein data.

## Funding support

This work is the result of NIH funding, in whole or in part, and is subject to the NIH Public Access Policy. Through acceptance of this federal funding, the NIH has been given a right to make the work publicly available in PubMed Central.

- NIH grants R01AI163160 (to JSD), K24AI150991 (to JSD), and U19AI175089 (to TSH, JSD, and MCA).

## Acknowledgments

We acknowledge the Benaroya Research Institute Genomics Core (RRID:SCR\_026658) for use of its facilities to generate and process next-generation sequencing data.

Address correspondence to: Jason S. Debley, Center for Respiratory Biology and Therapeutics, Seattle Children's Research Institute, 1916 Boren Avenue, Seattle, Washington 98101, USA. Email: jsd@uw.edu.

- Jartti T, Gern JE. Role of viral infections in the development and exacerbation of asthma in children. *J Allergy Clin Immunol.* 2017;140(4):895–906.
- Khetsuriani N, et al. Prevalence of viral respiratory tract infections in children with asthma. *J Allergy Clin Immunol.* 2007;119(2):314–321.
- Contoli M, et al. Role of deficient type III interferon-lambda production in asthma exacerbations. *Nat Med.* 2006;12(9):1023–1026.
- Wark PAB, et al. Asthmatic bronchial epithelial cells have a deficient innate immune response to infection with rhinovirus. *J Exp Med.* 2005;201(6):937–947.
- Spann KM, et al. Viral and host factors determine innate immune responses in airway epithelial cells from children with wheeze and atopy. *Thorax.* 2014;69(10):918–925.
- Patel DA, et al. Interferon response and respiratory virus control are preserved in bronchial epithelial cells in asthma. *J Allergy Clin Immunol.* 2014;134(6):1402–1412.
- Bhakta NR, et al. IFN-stimulated gene expression, type 2 inflammation, and endoplasmic reticulum stress in asthma. *Am J Respir Crit Care Med.* 2018;197(3):313–324.
- Altman MC, et al. Interferon response to respiratory syncytial virus by bronchial epithelium from children with asthma is inversely correlated with pulmonary function. *J Allergy Clin Immunol.* 2018;142(2):451–459.
- Altman MC, et al. Transcriptome networks identify mechanisms of viral and nonviral asthma exacerbations in children. *Nat Immunol.* 2019;20(5):637–651.
- Gaberino CL, et al. Dysregulation of airway and systemic interferon responses promotes asthma exacerbations in urban children. *J Allergy Clin Immunol.* 2025;155(5):1499–1509.
- Reddel HK, et al. An official American Thoracic Society/European Respiratory Society statement: asthma control and exacerbations: standardizing endpoints for clinical asthma trials and clinical practice. *Am J Respir Crit Care Med.* 2009;180(1):59–99.
- Jayavelu ND, et al. Type 2 inflammation reduces SARS-CoV-2 replication in the airway epithelium in allergic asthma through functional alteration of ciliated epithelial cells. *J Allergy Clin Immunol.* 2023;152(1):56–67.
- Ziegler CGK, et al. Impaired local intrinsic immunity to SARS-CoV-2 infection in severe COVID-19. *Cell.* 2021;184(18):4713–4733.
- Ordovas-Montanes J, et al. Allergic inflammatory memory in human respiratory epithelial progenitor cells. *Nature.* 2018;560(7720):649–654.
- Hewitt RJ, Lloyd CM. Regulation of immune responses by the airway epithelial cell landscape. *Nat Rev Immunol.* 2021;21(6):347–362.
- Jackson ND, et al. Single-cell and population transcriptomics reveal pan-epithelial remodeling in type 2-high asthma. *Cell Rep.* 2020;32(1):107872.
- Radzikowska U, et al. Rhinovirus-induced epithelial RIG-I inflammasome suppresses antiviral immunity and promotes inflammation in asthma and COVID-19. *Nat Commun.* 2023;14(1):2329.
- Zhu J, et al. Bronchial mucosal IFN- $\alpha/\beta$  and pattern recognition receptor expression in patients with experimental rhinovirus-induced asthma exacerbations. *J Allergy Clin Immunol.* 2019;143(1):114–125.
- Ghebre MA, et al. Severe exacerbations in moderate-to-severe asthmatics are associated with increased pro-inflammatory and type 1 mediators in sputum and serum. *BMC Pulm Med.* 2019;19(1):144.
- Niessen NM, et al. Sputum TNF markers are increased in neutrophilic and severe asthma and are reduced by azithromycin treatment. *Allergy.* 2021;76(7):2090–2101.
- Ray A, Kolls JK. Neutrophilic inflammation in asthma and association with disease severity. *Trends Immunol.* 2017;38(12):942–954.
- Lee JW, et al. Differential regulation of chemokines by IL-17 in colonic epithelial cells. *J Immunol.* 2008;181(9):6536–6545.
- Kolls JK, Lindén A. Interleukin-17 family members and inflammation. *Immunity.* 2004;21(4):467–476.
- Steinke JW, et al. Bronchoalveolar lavage cytokine patterns in children with severe neutrophilic and paucigranulocytic asthma. *J Allergy Clin Immunol.* 2021;147(2):686–693.
- Liu W, et al. Mechanism of T<sub>H</sub>2/T<sub>H</sub>17-predominant and neutrophilic T<sub>H</sub>2/T<sub>H</sub>17-low subtypes of asthma. *J Allergy Clin Immunol.* 2017;139(5):1548–1558.
- Brandt EB, et al. Diesel exhaust particle induction of IL-17A contributes to severe asthma. *J Allergy Clin Immunol.* 2013;132(5):1194–1204.
- Murphy RC, et al. Management strategies to reduce exacerbations in non-T2 asthma. *J Allergy Clin Immunol Pract.* 2021;9(7):2588–2597.

28. Wenzel SE, et al. A randomized, double-blind, placebo-controlled study of tumor necrosis factor- $\alpha$  blockade in severe persistent asthma. *Am J Respir Crit Care Med.* 2009;179(7):549–558.
29. Busse WW, et al. Randomized, double-blind, placebo-controlled study of brodalumab, a human anti-IL-17 receptor monoclonal antibody, in moderate to severe asthma. *Am J Respir Crit Care Med.* 2013;188(11):1294–1302.
30. Kim SR, et al. Endoplasmic reticulum stress influences bronchial asthma pathogenesis by modulating nuclear factor  $\kappa$ B activation. *J Allergy Clin Immunol.* 2013;132(6):1397–1408.
31. Pathinayake PS, et al. Understanding the unfolded protein response in the pathogenesis of asthma. *Front Immunol.* 2018;9:175.
32. Dastghaib S, et al. Mechanisms targeting the unfolded protein response in asthma. *Am J Respir Cell Mol Biol.* 2021;64(1):29–38.
33. Hur GY, Broide DH. Genes and pathways regulating decline in lung function and airway remodeling in asthma. *Allergy Asthma Immunol Res.* 2019;11(5):604–621.
34. Martino MB, et al. The ER stress transducer IRE1 $\beta$  is required for airway epithelial mucin production. *Mucosal Immunol.* 2013;6(3):639–654.
35. Hassan IH, et al. Influenza A viral replication is blocked by inhibition of the inositol-requiring enzyme 1 (IRE1) stress pathway. *J Biol Chem.* 2012;287(7):4679–4689.
36. Deprez M, et al. A single-cell atlas of the human healthy airways. *Am J Respir Crit Care Med.* 2020;202(12):1636–1645.
37. Morin A, et al. A functional genomics pipeline to identify high-value asthma and allergy CpGs in the human methylome. *J Allergy Clin Immunol.* 2023;151(6):1609–1621.
38. Djeddi S, et al. Rhinovirus infection of airway epithelial cells uncovers the non-ciliated subset as a likely driver of genetic risk to childhood-onset asthma. *Cell Genom.* 2024;4(9):100636.
39. Thompson EE, et al. Genetic contributions to epigenetic-defined endotypes of allergic phenotypes in children. *Am J Hum Genet.* 2025;112(7):1610–1624.
40. Djukanović R, et al. The effect of inhaled IFN- $\beta$  on worsening of asthma symptoms caused by viral infections. A randomized trial. *Am J Respir Crit Care Med.* 2014;190(2):145–154.
41. Jackson DJ. Inhaled interferon: a novel treatment for virus-induced asthma? *Am J Respir Crit Care Med.* 2014;190(2):123–124.
42. Lane C, et al. The use of non-bronchoscopic brushings to study the paediatric airway. *Respir Res.* 2005;6(1):53.
43. Lopez-Guisa JM, et al. Airway epithelial cells from asthmatic children differentially express proremodeling factors. *J Allergy Clin Immunol.* 2012;129(4):990–997.
44. Reeves SR, et al. Asthmatic airway epithelial cells differentially regulate fibroblast expression of extracellular matrix components. *J Allergy Clin Immunol.* 2014;134(3):663–670.
45. James RG, et al. Deficient follistatin-like 3 secretion by asthmatic airway epithelium impairs fibroblast regulation and fibroblast-to-myofibroblast transition. *Am J Respir Cell Mol Biol.* 2018;59(1):104–113.
46. Reeves SR, et al. Stability of gene expression by primary bronchial epithelial cells over increasing passage number. *BMC Pulm Med.* 2018;18(1):91.
47. Graham BL, et al. Standardization of spirometry 2019 update. An official American Thoracic Society and European Respiratory Society technical statement. *Am J Respir Crit Care Med.* 2019;200(8):e70–e88.
48. Bowerman C, et al. A race-neutral approach to the interpretation of lung function measurements. *Am J Respir Crit Care Med.* 2023;207(6):768–774.
49. Dweik RA, et al. An official ATS clinical practice guideline: interpretation of exhaled nitric oxide levels (FENO) for clinical applications. *Am J Respir Crit Care Med.* 2011;184(5):602–615.
50. Bochkov YA, et al. Improved molecular typing assay for rhinovirus species A, B, and C. *J Clin Microbiol.* 2014;52(7):2461–2471.
51. Hao Y, et al. Dictionary learning for integrative, multimodal and scalable single-cell analysis. *Nat Biotechnol.* 2024;42(2):293–304.
52. Dill-McFarland KA, et al. Kimma: flexible linear mixed effects modeling with kinship covariance for RNA-seq data. *Bioinformatics.* 2023;39(5):btad279.
53. Lun A, et al. EmptyDrops: distinguishing cells from empty droplets in droplet-based single-cell RNA sequencing data. *Genome Biol* 20, 63 (2019). <https://doi.org/10.1186/s13059-019-1662-y>